

# Local electric field enhancement at the heterojunction of Si/SiGe axially heterostructured nanowires under laser illumination

Jose Luis Pura<sup>1</sup>, Julián Anaya<sup>2</sup>‡, Jorge Souto<sup>1</sup>, Ángel Carmelo Prieto<sup>1</sup>, Andrés Rodríguez<sup>3</sup>, Tomás Rodríguez<sup>3</sup>, Juan Jiménez<sup>1</sup>

<sup>1</sup>GdS Optronlab, Dpt. Física de la Materia Condensada, ed. i+d, Parque Científico, Universidad de Valladolid, Paseo de Belén 1, 47011 Valladolid, Spain

<sup>2</sup>Centre for Device Thermography and Reliability, HH Wills Physics Laboratory, University of Bristol, Tyndall Avenue, BS8 1TL, Bristol, UK

<sup>3</sup>Ingeniería Electrónica, ETSI de Telecomunicación, Universidad Politécnica de Madrid, Avenida Complutense 30, 28040 Madrid, Spain.

## Abstract.

We present a phenomenon concerning the electric field enhancement at the heterojunction region of axially heterostructured Si/SiGe nanowires when the nanowire is illuminated by a focused laser beam. The electric field is sensed by micro Raman spectroscopy, which permits to reveal the enhancement of the Raman signal arising from the heterojunction region; the Raman signal per unit volume increases at least 10 times with respect to the homogeneous Si, and SiGe nanowire segments. In order to explore the physical meaning of this phenomenon, a 3-dimensional solution of the Maxwell equations of the interaction between the focused laser beam and the nanowire was carried out by finite element methods. A local enhancement of the electric field at the heterojunction was deduced; however, the magnitude of the electromagnetic field enhancement only approaches the experimental one when the free carriers are considered, showing enhanced absorption at the carrier depleted heterojunction region. The existence of this effect promises a way to improve the photon harvesting using axially heterostructured semiconductor NWs.

## 1. Introduction

Semiconductor nanowires (NWs) are attracting a great deal of attention because of the increasing number of potential applications based on their unique properties.[1] Most of these properties arise from the NW confined dimension, the diameter, as compared to some characteristic lengths, e.g. exciton Bohr radius, phonon mean free path, wavelength of the incident electromagnetic (EM) waves, etc.[2] In particular, there is a great interest in the interaction between semiconductor NWs and light,

‡ Corresponding Author

as their optical properties make of them the optimal candidates for nanophotonic devices.[3][4] A broad range of unique optical properties of semiconductor NWs have been reported, e.g. waveguiding,[5] optical resonances,[6] antenna effects among others.[7] All these effects emerge because light interacts with the NWs in different ways depending on the NW diameter, wavelength, and dielectric properties of the NW and the surrounding media. One of the most relevant properties concerning the light/NW interaction is the ability of NWs to enhance their optical absorption/scattering for certain diameters, which are characterized by large local electric fields inside the NW.[8] The absorption/scattering resonances deal with different phenomena recently reported, including, among other, the enhanced photocurrent response of the NWs,[7] enhanced elastic and inelastic light scattering by Si NWs,[9] light extinction,[10] light emission in different semiconductor NWs,[11][12] and second harmonic generation.[5] Since the Raman intensity is proportional to the excitation light intensity and the scattering volume, the experimental study of the interaction of light with matter at the nanoscale can be carried out by its Raman response.[13] This makes of Raman spectroscopy an excellent probe for sensing the local electric field induced inside the NW under incident light. In addition, it is possible to take advantage of its capabilities as a powerful non-destructive technique for the characterization of the structure, composition, stress, thermal, electronic, and optical properties of semiconductor NWs.[6][14][15][16][17][18] It is worth noting that up to now the research interest about the light/NWs interaction has been focused mainly on homogeneous single NWs and/or core-shell heterostructured NWs;[19] however, the response of axially heterostructured NWs to the electromagnetic waves is still unexplored. These kind of structures are attracting an increasing interest since heterojunctions (HJ) are necessary for the development of semiconductor NW based devices.[20] In the junction of these NWs a jump in the complex refractive index due the abrupt change of materials is expected, which therefore may change the electromagnetic (EM) response of the NW. Besides the HJ built-in electric field, which can locally change the polarizability, the oscillator strength and the presence of free carriers, either native or photogenerated, could also affect the electric field distribution inside the NW. To further advance in this subject, we present in this work a study of the distribution of the electromagnetic field in axially heterostructured Si/SiGe NWs, paying special attention to the role of the HJ in the optical response of the NW. This is carried out experimentally by using its Raman response as a sensor of the local electric field. The experimental data are compared to the output of a 3 dimensional (3D) solution of the Maxwell equations characterizing the electromagnetic laser/NW interaction by finite element methods (EM-FE), enabling to explain the role of the HJ in the EM interaction.

## 2. Experimental description and samples

Axially-heterostructured NWs were grown by the vapour-liquid-solid (VLS) method, using  $Si_2H_6$  and  $GeH_4$  as precursor gases and alloyed Ga-Au metal droplets of different

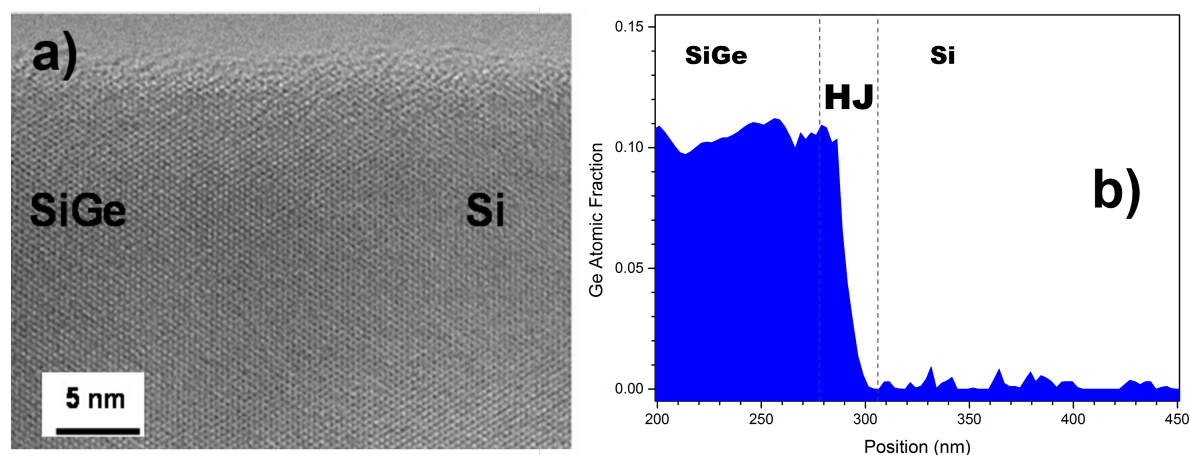


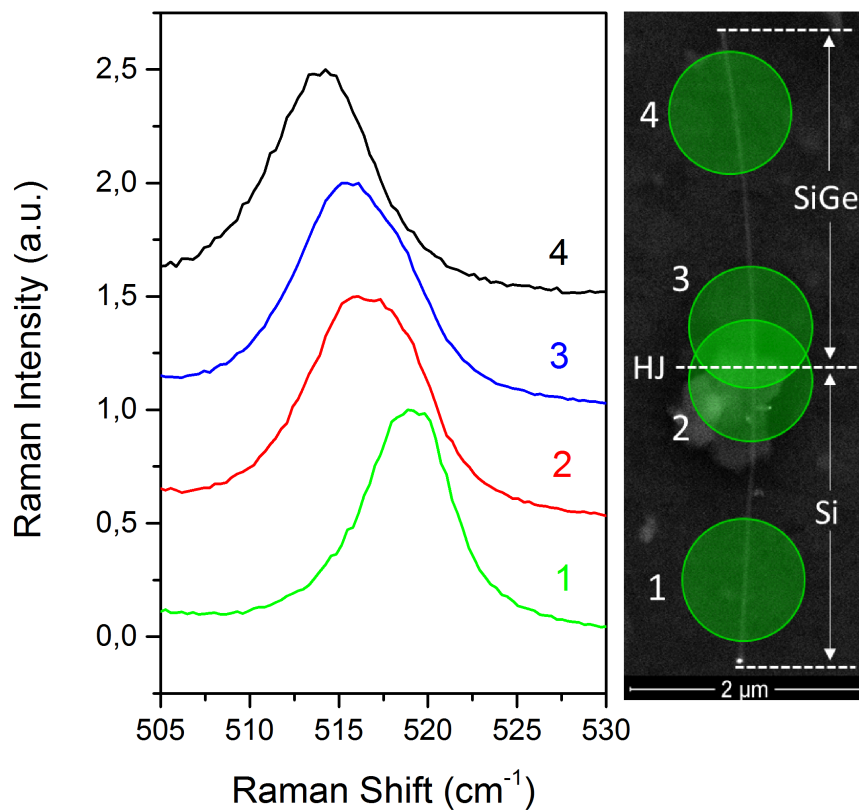
**Figure 1.** a) High resolution TEM image of the HJ. b) EDX Ge atomic fraction profile across the HJ.

compositions as catalysts. The as-grown NWs were sonicated in an ultrasonic bath and suspended in methanol; subsequently the NWs were deposited on an Al substrate by drop-casting. For more details about the growth of these NWs see refs [21] and [22]. High resolution transmission electron microscopy (TEM) and energy dispersive X ray (EDX) analyses of the HJ was carried out. High resolution TEM images of the HJ region of SiGe/Si HJs did not show structural discontinuities at the junction, nor stacking faults, or other structural defects, Fig.1a. The EDX profile shows a compositionally graded HJ with a width of around 30 nm, of the order of the NW diameter,  $\approx 32$  nm for the NW shown in Fig. 1b.

The micro Raman spectra of several individual Si/SiGe NWs were recorded with a high resolution Labram UV-HR 800 Raman spectrometer from Horiba-JovinYvon. The excitation and the scattered light collection were performed by means of a confocal metallographic microscope with a high magnification objective (100X and 0.95 numerical aperture (NA)). The excitation was done with a frequency doubled Nd:YAG laser (532 nm). The measured laser beam diameter at the focal plane for these conditions is  $\sim 1 \mu\text{m}$ , thus slightly bigger than the  $\sim 700$  nm given by the Abbe's criteria ( $w_0 \propto 1.22\lambda/NA$ ) and several times larger than the typical NW diameter studied here, which range from 40 to 100 nm. The NWs deposited on a metallic substrate were found to enhance the Raman signal with respect to the free standing NWs. The metallic substrate also allows a better heat dissipation, reducing the laser induced heating of the NWs.[23] The Ge concentration in the SiGe segment of the NW, measured by EDX and confirmed by the Raman measurements, lies around 10% for all the studied NWs. Prior to the Raman measurements the dimensions and morphology of the NWs were characterized in a scanning electron microscope (SEM). The Raman spectra were acquired by scanning the laser beam along and across the NW axis in steps of 100 nm. The transverse scanning across the NW allows the optimization of the excitation conditions, i.e. maximum Raman signal with negligible laser induced heating.[23] The longitudinal scanning

permits to localize the HJ, and also to study the Raman intensity profiles along the NW, and more interestingly around the HJ.

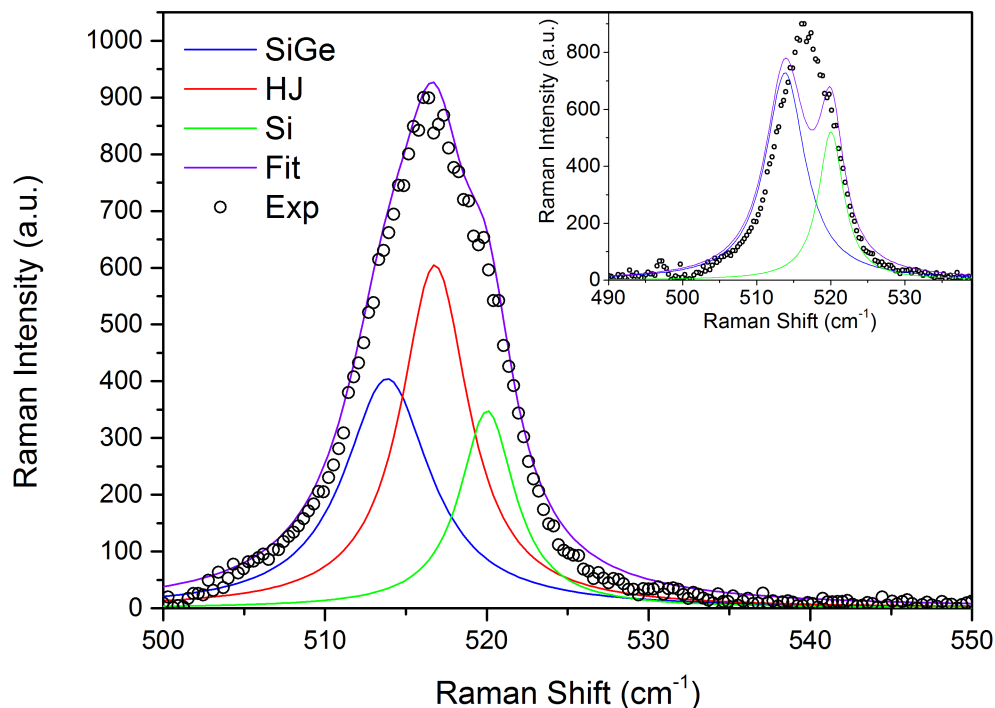
### 3. Experimental results



**Figure 2.** Raman spectra recorded at different positions along the heterostructured Si/SiGe NW. The positions of the laser spot along the NW are indicated in the SEM image. Spectrum 1 is taken on the Si segment, spectra 2 and 3 share the three regions of the NW and spectrum 4 is taken on the SiGe segment.

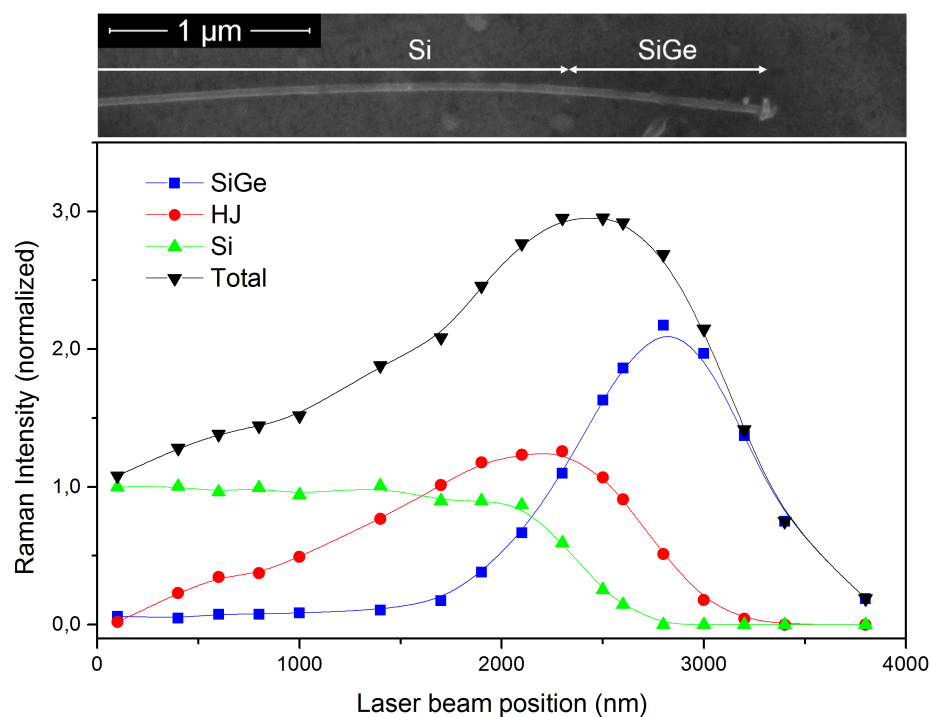
Four Raman spectra recorded at different positions along an axially heterostructured Si/SiGe NW are shown in Figure 2. Spectrum 1 was taken on the Si segment of the NW, while spectrum 4 was recorded on the SiGe segment. Spectra 2 and 3 were recorded with the laser beam sharing the two pure segments and the HJ. When these spectra are compared, a dramatic change is observed in the spectral shape of 2 and 3 with respect to 1 and 4. Spectra 1 and 4 show a typical Lorentzian peak, with the spectral parameters characteristic of Si and  $Si_{0.9}Ge_{0.1}$  NWs respectively.[24][25] Meanwhile, the spectra recorded in positions 2 and 3 appear broadened and asymmetric, as a consequence of the overlapping contribution to the Raman spectrum of the different regions of the NW being simultaneously excited by the laser beam. In order to analyze this signal, spectral deconvolution shall be thus carried out to ascertain the different contributions of the pure Si and SiGe segments of the NW, and also the contribution of the HJ region. For this deconvolution we used the spectra 1 and 4, corresponding unequivocally to the Si and  $Si_{0.9}Ge_{0.1}$  pure NW segments, as the reference spectra for the fitting of the spectra 2 and 3. However when using a weighted Gaussian convolution –from the focused laser intensity distribution– of the two bands corresponding to the two pure segments it is not possible to reproduce the Raman recorded when the laser beam is sharing the three NW regions, i.e. spectra 2 and 3 (see Fig.3 inset).

Fig. 3 shows that a third band is necessary to achieve a satisfactory fit of the spectra recorded with the participation of the HJ, e.g. 2 and 3. This third contribution, which has a peak width and frequency intermediate between those recorded for the pure Si and  $Si_{0.9}Ge_{0.1}$  NW segments, should arise exclusively from the very narrow HJ region. It should be noted that the HJ region in VLS NW growth does not present a sharp composition change, but it follows a compositionally graded transition from the nominal 10% Ge of the SiGe segment to the pure Si segment (see Fig.1a). The thickness of this transition region is of the same order of magnitude of the NW diameter, and it is consequence of the Ge reservoir effect on the catalyst droplet. Once the  $GeH_4$  gas source had been switched-off this reservoir continues depositing Ge during the growth up to the Ge exhaustion in the catalysts droplet.[3] [26][27] Thus, in order to explain the Raman signal detected in the HJ region, we should first consider this transition volume as the source of the observed third band in the Raman spectrum. The Raman intensity is correlated to the volume of the material probed by the laser beam,[14] which in our case gives a ratio of  $\sim 1:0.1:1$  (Si:HJ:SiGe) between the three probed regions for a 50 nm diameter NW when the laser beam spot is sharing the three parts of the NW (when it is centered around the HJ). Therefore, the high intensity of the Raman band arising from the HJ region (see Fig. 3), which is similar in amplitude to the ones corresponding to the Si and SiGe NW segments, cannot be explained in terms of a simple convolution of the signals weighted by their scattering volumes. Indeed, the high intensity recorded in the HJ when translated in terms of Raman intensity per unit volume, results in a Raman signal enhancement for the HJ contribution of at least one order of magnitude with respect to the signals recorded in the two single NWs segments. This means that there is a significant enhancement of the induced local electric field at the HJ of the NW.



**Figure 3.** Fitting of the Raman signal corresponding to an intermediate composition between the two NW segments, a satisfactory fitting can only be achieved by using a third Raman band. (Inset) Fitting of a Raman spectrum sharing the three NW regions using only two bands with the spectral parameters of the Raman bands of the pure Si and SiGe segments respectively, this fitting neglects the contribution of the HJ.

Furthermore, the Raman intensity along the heterostructured NW is not only amplified at the HJ, but the presence of the HJ seems to pull up of the overall Raman signal. This is shown in Fig. 4, in which the integrated Raman intensities of the different contributions, - namely Si, HJ and SiGe- as determined from the deconvolution of the experimental Raman spectra are plotted as a function of the position of the laser beam along the NW. Here the Raman intensity reaches a maximum when the laser beam is crossing the HJ, evidencing that the presence of the HJ is enhancing the overall Raman intensity, and thus affecting the distribution of the electric field inside the NW even when the laser beam is not directly illuminating the HJ. We should note that this behavior was observed for all of the several axially heterostructured NWs that we have studied. On the other hand, the decrease of the SiGe signal at the right side of the plot of Fig. 4 is the consequence of the reduced scattering volume and Gaussian intensity profile of the laser at the end of the NW (see the SEM image of Fig.4). The same effect occurs on the other end of the NW (Si segment) but it is not plotted here.



**Figure 4.** Intensity profiles along the NW axis for the overall Raman signal and for the deconvoluted bands corresponding to the three regions of the NW, showing the enhancement under the influence of the HJ. The points correspond to the positions of the laser beam center where the Raman spectra were recorded. The data have been normalized to the one corresponding to the pure Si region to better illustrate the enhancement in Raman signal.

#### 4. Laser/NW interaction by finite element method (EM-FEM) simulations

To study the quantitative interaction between the focused laser beam and the NWs, and thus to unravel the distribution of the electromagnetic field inside the HJ NW, one needs to solve the Maxwell equations for the laser/NW system. This has been typically carried out by means of the Lorenz-Mie theory, in which the NW is described as an infinitely long cylinder immersed in a homogeneous and isotropic non absorbing medium.[28] In the frame of this formalism, the calculation of the absorption, and scattering efficiencies,  $Q_{abs}$  and  $Q_{sc}$  respectively, has revealed a strong dependence of these coefficients with the NW diameter, presenting resonances for certain diameters.[6][17] Alternatively, we have analyzed the NW/laser beam interaction by solving the equivalent 2D Maxwell equations using the radio-frequency (RF) module of the COMSOL Multiphysics simulation software, contrasting our results with the solution of the Lorentz-Mie equations and obtaining an excellent agreement.[29] However, because of symmetry-breaking in the

presence of the HJ, the simulation of the axially heterostructured NWs cannot be performed by a 2D approach like the ones typically used when studying the light/NW interaction for homogeneous NWs and core-shell heterostructured NWs.[14][15] Instead, here we solved a 3D model accounting for the axial HJ and the finite length of the NW, as well as the presence of the metallic substrate. The electromagnetic model used here reproduces a HJ-NW with the same characteristics as the one shown in Fig. 4, deposited on a metallic (Al) substrate and surrounded by air. The NW is illuminated by the same 532 nm Gaussian laser beam used in the experiments. The air/NW/substrate system was limited by Cartesian perfectly matched layers (PMLs), which absorb all the outgoing radiation, thus eliminating secondary reflections on the boundaries. The complex refractive indexes were obtained from Sopra database.[30] In a first step the response of a perfectly dielectric NW was calculated. This model was solved for different positions of the excitation laser beam along the NW axis in order to reproduce the experimental profile of Fig. 4. A particular solution of the model is shown in Fig.5, where one observes the 3D distribution of the relative electric field intensity, defined as  $E_r^2 = |E|^2/|E_{Incident}|^2$  (i.e., the electric field enhancement over the incident laser electromagnetic field), inside the heterostructured NW. In the same figure we also included the profile of this magnitude along the NW axis, highlighting the local enhancement at the HJ region. For each position of the laser beam the electromagnetic field distribution inside the NW is calculated. The volume integrals of the square of the electric field,  $|E|^2$ , in the three different regions: Si segment, SiGe segment and the HJ, are then calculated. The value of these integrals should therefore be proportional to the theoretical Raman signal arising from each NW region under the excitation beam.[13] It is remarkable that this model shows a similar amplification and localization of the EM field in the HJ region, see Fig.5; however, the estimated amplification for the HJ region was lower than the one deduced from the experimental data (see Fig 6, pink dots). In order to explain this discrepancy, a more complete model accounting for the effect of the photogenerated carriers in the solution of the Maxwell equations was considered. This is needed since the presence of free carriers will contribute to the dielectric losses. For the excitation conditions of our measurements and a surface recombination velocity (SRV) of  $S \approx 3 \cdot 10^5 \text{ cm/s}$ ,[31] it results in a photogenerated carrier concentration of  $n \approx 10^{19} \text{ cm}^{-3}$ , in agreement with other experimental estimations.[31] The dielectric losses will mainly affect the regions with free carriers, i.e. the two NW segments; but as a consequence of the carrier depletion at the HJ, this region will be free of the losses associated with the presence of free carriers. As a result, the dielectric losses will modify the electric field distribution inside the NW, lowering the electric field in the homogeneous segments with respect to the HJ, which yields an effective amplification of the HJ signal.

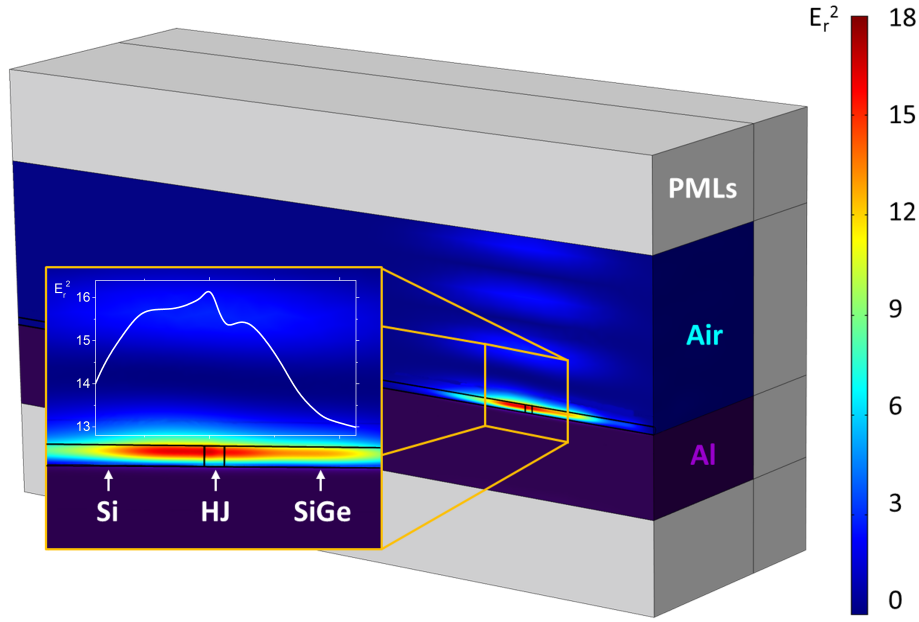


**Figure 5.** 3D representation of a solution of the model for a similar heterostructured NW than the ones experimentally studied. A magnification of the HJ region with the  $E_r^2$  relative intensity axial profile showing enhancement at the HJ is also represented.

Once the free carriers were considered the model was solved for a carrier density ranging from  $10^{16}$  to  $10^{20} \text{cm}^{-3}$ . The results obtained for two representative carrier densities,  $n = 8 \cdot 10^{18} \text{cm}^{-3}$  and  $n = 5 \cdot 10^{19} \text{cm}^{-3}$ , are shown in Fig. 6. From here it is clear that by including the effect of the photogenerated carriers in the model, the electric field is strongly localised in the HJ region, well approaching the contribution observed in the experimental data of Fig.4, and therefore explaining the origin of anomalous effect observed in the experiments. However we should note that the experimental intensity of the SiGe segment is higher than the intensity measured for the Si segment, as opposed to what is observed in the EM-FEM model, which shows similar values for both segments. This discrepancy might arise by a difference of a few nanometers in the diameter of both segments, which due the diameter dependent resonance in the Raman intensity, can be responsible for the observed difference;[29]in fact, diameter changes in the presence of axial HJs are common. Here to simplify the problem, the data of Fig. 6 were calculated for an ideal cylindrical NW, without diameter change and therefore the model do not account for these subtle differences in geometry.

Finally, and to fully validate the model, the hypothesis of including the photogenerated carriers as an important player to explain the observed Raman intensity needs to be tested experimentally. In nanoscale systems the photogenerated carrier concentration is dominated by the surface recombination; therefore, by modifying the surface condition, one can change the surface recombination velocity (SRV) which in return will induce a change in the free carrier density. Taking this into account, Si NWs were dipped in a 4% HF solution in order to remove the native oxide layer, changing

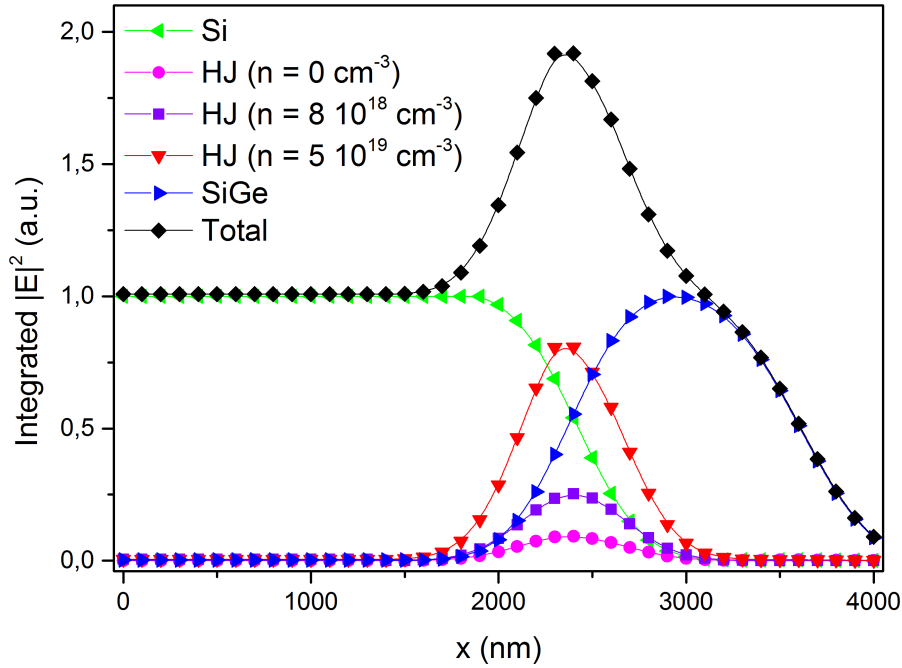


**Figure 6.** Integrated values of  $|E|^2$  (proportional to the Raman signal) along a NW with the same compositional and geometrical properties as the NW of Fig.4. Results are shown for a perfectly dielectric NW ( $n = 0$ ), and two different carrier densities. The calculated total signal corresponds to  $n = 5 \cdot 10^{19} \text{ cm}^{-3}$ .

their SRV. The chemical treatment removes the native  $\text{SiO}_2$  external layer and does not react with the crystalline Si core, leaving a clean Si NW. The NWs were immediately deposited in the metallic substrate, and kept in a  $\text{N}_2$  atmosphere up to the first Raman measurement. After this point the  $\text{N}_2$  source is switched off and the oxidation process starts at room temperature. Immediately after the removal of the oxide layer the surface recombination states will be nearly suppressed, then the equilibrium photogenerated carrier density will raise, lowering the Raman signal because of the free carrier associated losses. As time goes on and the spontaneous oxidation process takes place, new surface recombination centers are created and the SRV increases, with the reduction of the free carrier density and the concomitant increase of the Raman signal. In our experiment, the Raman spectrum was periodically recorded for one week of measurements, albeit the Raman signal became fully stable after the second day. The Raman signal evolution for this Si NW can be seen in Fig. 7, showing that the intensity is starting to reach a stable value after the first 24 hours. This is in good agreement with the time needed for the formation of the first stable oxide layer in Si at room temperature, which lies around 25-30 hours.[32] This therefore shows the evolution of the Raman signal with the change of the SRV, which progressively increased due to the oxidation. It should be noted that this experimental configuration warrants the same excitation conditions

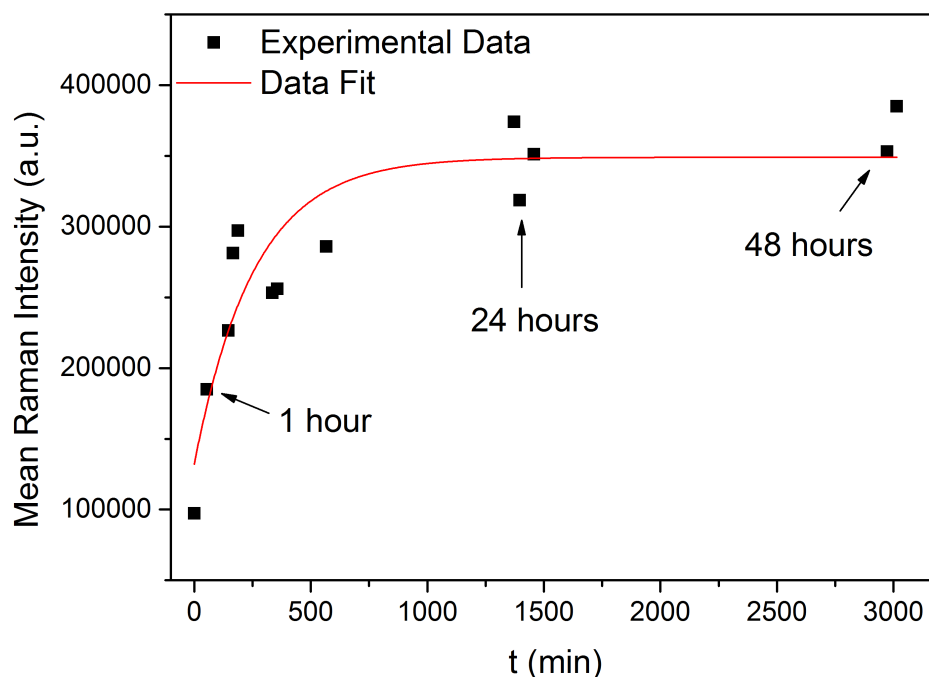


**Figure 7.** Evolution of the mean Raman Intensity of a Si NW as a function of the oxidation time. The intensity becomes stable 25-30 hours after the oxidation began, which coincides with the formation of the first stable oxide layer.[32]

and photogeneration rate for all the measurements and thus shows that the change in the photogenerated carrier concentration is controlled by the SRV. Besides, the Raman signal raises rather fast in the first hours of oxidation, suggesting that the creation of a full oxide layer is not needed to enhance the surface recombination, but the creation of sparse defects at the surface is enough to spoil the homogeneity of the Si surface, and create surface states. With the presence of surface states, the equilibrium photo-carrier concentration decreases and the Raman signal is progressively recovered. Therefore this result highlights the role played by the free carriers in the laser/NW interaction, and supports the good agreement observed between theoretical and experimental results obtained in the heterostructured NWs when the photogenerated carriers are considered in the electromagnetic interaction.

## 5. Summary

We have presented here a local electromagnetic amplification phenomenon in the HJ region of axially heterostructured Si/SiGe NWs when interacting with a laser beam. This nanoscale effect has been systematically studied by recording the Raman signals of the heterostructured NWs, which show a significant enhancement at the HJ region with respect to those obtained in compositionally homogeneous NWs of the same dimensions.

The Raman intensity of the HJ presents an intensity per unit volume at least 10 times higher than the pure segments of the NW. These experimental observations were contrasted with the results obtained by the 3D solution of the Maxwell equations for the interaction between the dielectric NW and the focused laser beam using an EM-FEM model. The model accounts for the above experimental observations, and shows the possibility of locally modify the electric field in the HJ; however, the calculated electric field enhancement at the HJ is substantially lower than the one observed experimentally by the Raman signal. A further improvement of the model considering the contribution of the photogenerated free carriers improves the calculated values up to the experimental observations. The role of the photogenerated carriers in the Raman response of the NWs has been revealed by experiments changing the photocarrier recombination dynamics by modifying the surface recombination velocity. The local electric field inside the NW can be modulated by the presence of the HJ and the surface states. This electromagnetic field enhancement at the HJ of axially heterostructured NWs suggests a path to optimize light-sensitive devices as photodetectors, sensors, solar cells, among other.

## Acknowledgments

This work was funded by Junta de Castilla y Len (Project VA293U13), Spanish Government (CICYT MAT2010-20441-C02 (01 and 02)) and FEDER (MINECO - ENE 2014-56069-C4-4-R) . J.L. Pura was granted by the FPU programme (Spanish Government)(FPU14/00916. We also acknowledge Prof. C.Ballesteros (Universidad Carlos III, Madrid) for providing the EDX and TEM results.

## Bibliography

- [1] Cui Y and Lieber C M 2001 *Science* **291** 851–853 ISSN 0036-8075 (*Preprint* <http://science.sciencemag.org/content/291/5505/851.full.pdf>) URL <http://science.sciencemag.org/content/291/5505/851>
- [2] Rurali R 2010 *Rev. Mod. Phys.* **82**(1) 427–449 URL <http://link.aps.org/doi/10.1103/RevModPhys.82.427>
- [3] Yan R, Gargas D and Yang P 2009 *Nat Photon* **3** 569–576 ISSN 1749-4885 URL <http://dx.doi.org/10.1038/nphoton.2009.184>
- [4] Loitsch B, Rudolph D, Morkötter S, Döblinger M, Grimaldi G, Hanschke L, Matich S, Parzinger E, Wurstbauer U, Abstreiter G, Finley J J and Koblmüller G 2015 *Advanced Materials* **27** 2195–2202 ISSN 1521-4095 URL <http://dx.doi.org/10.1002/adma.201404900>
- [5] Law M, Sirbuluy D J, Johnson J C, Goldberger J, Saykally R J and Yang P 2004 *Science* **305** 1269–1273 ISSN 0036-8075 (*Preprint* <http://science.sciencemag.org/content/305/5688/1269.full.pdf>) URL <http://science.sciencemag.org/content/305/5688/1269>
- [6] Kallel H, Arbouet A, BenAssayag G, Chehaidar A, Potié A, Salem B, Baron T and Paillard V 2012 *Phys. Rev. B* **86**(8) 085318 URL <http://link.aps.org/doi/10.1103/PhysRevB.86.085318>
- [7] Cao L, Fan P, Vasudev A P, White J S, Yu Z, Cai W, Schuller J A, Fan S and Brongersma M L 2010 *Nano Letters* **10** 439–445 pMID: 20078065 (*Preprint* <http://dx.doi.org/10.1021/nl9036627>) URL <http://dx.doi.org/10.1021/nl9036627>
- [8] Ruppini R 1998 *J. Opt. Soc. Am. A* **15** 1891–1895 URL <http://josaa.osa.org/abstract.cfm?URI=josaa-15-7-1891>

- [9] Cao L, Fan P, Barnard E S, Brown A M and Brongersma M L 2010 *Nano Letters* **10** 2649–2654 pMID: 20507083 URL <http://dx.doi.org/10.1021/nl1013794>
- [10] Schuller J A, Zia R, Taubner T and Brongersma M L 2007 *Phys. Rev. Lett.* **99**(10) 107401 URL <http://link.aps.org/doi/10.1103/PhysRevLett.99.107401>
- [11] Nobis T, Kaidashev E M, Rahm A, Lorenz M and Grundmann M 2004 *Phys. Rev. Lett.* **93**(10) 103903 URL <http://link.aps.org/doi/10.1103/PhysRevLett.93.103903>
- [12] van Dam D, Abujetas D R, Paniagua-Domínguez R, Sánchez-Gil J A, Bakkers E P A M, Haverkort J E M and Rivas J G 2015 *Nano Letters* **15** 4557–4563 pMID: 26043200 (*Preprint* <http://dx.doi.org/10.1021/acs.nanolett.5b01135>) URL <http://dx.doi.org/10.1021/acs.nanolett.5b01135>
- [13] Aussenegg F R and Lippitsch M E 1986 *Journal of Raman Spectroscopy* **17** 45–49 ISSN 1097-4555 URL <http://dx.doi.org/10.1002/jrs.1250170110>
- [14] Lopez F J, Hyun J K, Givan U, Kim I S, Holsteen A L and Lauhon L J 2012 *Nano Letters* **12** 2266–2271 pMID: 22497202 (*Preprint* <http://dx.doi.org/10.1021/nl204537d>) URL <http://dx.doi.org/10.1021/nl204537d>
- [15] Xiong Q, Chen G, Gutierrez H and Eklund P 2006 *Applied Physics A* **85** 299–305 ISSN 1432-0630 URL <http://dx.doi.org/10.1007/s00339-006-3717-7>
- [16] Doerk G S, Carraro C and Maboudian R 2012 Raman spectroscopy for characterization of semiconducting nanowires *Raman Spectroscopy for Nanomaterials Characterization* (Springer) pp 477–506
- [17] Cao L, Nabet B and Spanier J E 2006 *Phys. Rev. Lett.* **96**(15) 157402 URL <http://link.aps.org/doi/10.1103/PhysRevLett.96.157402>
- [18] Torres A, Martín-Martín A, Martínez O, Prieto A C, Hortelano V, Jiménez J, Rodríguez A, Sangrador J and Rodríguez T 2010 *Applied Physics Letters* **96** 011904 URL <http://scitation.aip.org/content/aip/journal/apl/96/1/10.1063/1.3284647>
- [19] Lauhon L J, Gudiksen M S, Wang D and Lieber C M 2002 *Nature* **420** 57–61 ISSN 0028-0836 URL <http://dx.doi.org/10.1038/nature01141>
- [20] Le S T, Jannaty P, Luo X, Zaslavsky A, Perea D E, Dayeh S A and Picraux S T 2012 *Nano Letters* **12** 5850–5855 pMID: 23113718 (*Preprint* <http://dx.doi.org/10.1021/nl3032058>) URL <http://dx.doi.org/10.1021/nl3032058>
- [21] Rodríguez A, Sangrador J, Rodríguez T, Ballesteros C, Prieto C and Jiménez J 2010 *MRS Proceedings* **1258** 1258–P05–05 URL <http://dx.doi.org/10.1557/PROC-1258-P05-05>
- [22] Rodríguez A, Rodríguez T, Ballesteros C and Jiménez J 2013 *MRS Proceedings* **1510** mrsf12–1510–dd06–05 URL <http://dx.doi.org/10.1557/opl.2013.273>
- [23] Anaya J, Torres A, Hortelano V, Jiménez J, Prieto A C, Rodríguez A, Rodríguez T, Rogel R and Pichon L 2013 *Applied Physics A* **114** 1321–1331 ISSN 1432-0630 URL <http://dx.doi.org/10.1007/s00339-013-7966-y>
- [24] Alonso M I and Winer K 1989 *Phys. Rev. B* **39**(14) 10056–10062 URL <http://link.aps.org/doi/10.1103/PhysRevB.39.10056>
- [25] Pearsall T P 1989 *Critical Reviews in Solid State and Materials Sciences* **15** 551–600 (*Preprint* <http://dx.doi.org/10.1080/10408438908243745>) URL <http://dx.doi.org/10.1080/10408438908243745>
- [26] Periwal P, Sibirev N V, Patriarche G, Salem B, Bassani F, Dubrovskii V G and Baron T 2014 *Nano Letters* **14** 5140–5147 pMID: 25118977 (*Preprint* <http://dx.doi.org/10.1021/nl5019707>) URL <http://dx.doi.org/10.1021/nl5019707>
- [27] Clark T E, Nimmatoori P, Lew K K, Pan L, Redwing J M and Dickey E C 2008 *Nano Letters* **8** 1246–1252 pMID: 18321076 (*Preprint* <http://dx.doi.org/10.1021/nl072849k>) URL <http://dx.doi.org/10.1021/nl072849k>
- [28] Brønstrup G, Jahr N, Leiterer C, Csáki A, Fritzsche W and Christiansen S 2010 *ACS Nano* **4** 7113–7122 ISSN 1936-0851 URL <http://dx.doi.org/10.1021/nn101076t>
- [29] Anaya J, Jiménez J, Rodríguez A and Rodríguez T 2014 Electromagnetic interaction between a

laser beam and semiconductor nanowires deposited on different substrates: Raman enhancement in si nanowires *Symposium L, Photonic and Plasmonic Materials for Enhanced Optoelectronic Performance (MRS Proceedings vol 1627)*

- [30] SOPRA 2016 Sopra database URL <http://www.sspectra.com/sopra.html>
- [31] Sabbah A J and Riffe D M 2000 *Journal of Applied Physics* **88** 6954–6956 URL "<http://scitation.aip.org/content/aip/journal/jap/88/11/10.1063/1.1316047>"
- [32] Morita M, Ohmi T, Hasegawa E, Kawakami M and Ohwada M 1990 *Journal of Applied Physics* **68** 1272–1281 URL <http://scitation.aip.org/content/aip/journal/jap/68/3/10.1063/1.347181>